JAERI-M
9862

HEAT LOAD REDUCTION OF THE DIVERTOR PLATE AND FORMATION OF DENSE AND COLD DIVERTOR PLASMA BY REMOTE RADIATIVE COOLING IN DOUBLET-III AND INTOR

[IAEA INTOR Workshop Report, Phase IIA, Group B]

December 1981

Michiya SHIMADA, Masayuki NAGAMI, Kimihiro IOKI[*1],
Shigeru IZUMI[*2], Masaki MAENO, Hideaki YOKOMIZO
Kichiro SHINYA[*3], Hidetoshi YOSHIDA, N.H.BROOKS[*4]
C.L.HSIEH[*4], Akio KITSUNEZAKI and Noboru FUJISAWA

日本原子力研究所
Japan Atomic Energy Research Institute

JAERI-Mレポートは，日本原子力研究所が不定期に公刊している研究報告書です。
入手の問合わせは，日本原子力研究所技術情報部情報資料課（〒319-11茨城県那珂郡東海村）あて，お申しこしください。なお，このほかに財団法人原子力弘済会資料センター（〒319-11 茨城県那珂郡東海村日本原子力研究所内）で複写による実費頒布をおこなっております。

JAERI-M reports are issued irregularly.
Inquiries about availability of the reports should be addressed to Information Section, Division of Technical Information, Japan Atomic Energy Research Institute, Tokai-mura, Naka-gun, Ibaraki-ken 319-11, Japan.

編集兼発行　日本原子力研究所
印　　刷　㈱高野高速印刷

JAERI-M 9862

HEAT LOAD REDUCTION OF THE DIVERTOR PLATE AND FORMATION OF DENSE AND COLD DIVERTOR PLASMA BY REMOTE RADIATIVE COOLING IN DOUBLET-III AND INTOR

[IAEA INTOR Workshop Report, Phase IIA, Group B]

Michiya SHIMADA, Masayuki NAGAMI, Kimihiro IOKI[*1],
Shigeru IZUMI[*2], Masaki MAENO, Hideaki YOKOMIZO
Kichiro SHINYA[*3], Hidetoshi YOSHIDA, N.H. BROOKS[*4]
C.L. HSIEH[*4], Akio KITSUNEZAKI and Noboru FUJISAWA

Division of Large Tokamak Development,
Tokai Research Establishment, JAERI

(Received December 3, 1981)

The experimental results on remote radiative cooling in Doublet-III are summarized. The feasibility of remote radiative cooling is discussed for the case of INTOR.

Keywords: Doublet-III, INTOR, Divertor, Remote Radiative Cooling,
Heat Removal

This work was performed under a cooperative agreement between the Japan Atomic Energy Research Institute and the United States Department of Energy under DOE Contract No. DE-AT03-U0SF11512.

*1) On leave from Mitsubishi Atomic Power Industries, Inc.
*2) On leave from Hitachi Ltd.
*3) On leave from Tokyo Shibaura Electric Corporation
*4) General Atomic Company, San Diego, California, USA

JAERI-M 9862

ダブレットⅢとイントールにおける遠隔放射冷却による高密度低温ダイバータプラズマの形成とダイバータプレートへの熱負荷の軽減

〔IAEA INTOR Workshop Report Phase ⅡA, Group B〕

日本原子力研究所東海研究所大型トカマク開発部
嶋田　道也・永見　正幸・伊尾木公裕[*1]
出海　滋[*2]・前野　勝樹・横溝　英明
新谷　吉郎[*3]・吉田　英俊・N.H.BROOKS[*4]
C.L.HSIEH・狐崎　晶雄
藤沢　登

（１９８１年１２月３日受理）

ダブレットⅢでの遠隔放射冷却に関する実験結果を総括し，INTORでの遠隔放射冷却の可能性を論じる。

＊１）　外来研究員：三菱原子力工業（株）
＊２）　外来研究員：日立製作所（株）
＊３）　外来研究員：東京芝浦電気（株）
＊４）　General Atomic Co.

Contents

目　　次

1. INTRODUCTION

A natural single-null divertor configuration, which is obtained as a simple modification of D-shaped plasma cross sections in Doublet-III, demonstrated an impurity control capability without a divertor chamber and with the divertor coils outside the vacuum chamber [1]. The successful operation of this single-null poloidal divertor demonstrates some new advantages for a diverted tokamak in addition to the suppression of impurity influx as demonstrated in DIVA. In diverted discharges, plasma density and recycling at the divertor region is found to increase non-linearly with the increase of the main plasma density [2]. This results in a large radiation power density in the divertor region [3,4], and a large increase in the helium pressure in the divertor region [5]. The high helium pressure in the divertor facilitates the helium ash exhaust in fusion reactors. The strong radiative cooling possibly negates the heat removal and erosion problems of the divertor plate which are the major drawbacks of a diverted tokamak.

In Section 2, experimental results on remote radiative cooling [3,4] are summarized. A 1-D heat conduction simulation of the radiative divertor plasma elucidates the effect of radiative cooling in the formation of the dense and cold divertor plasma. The feasibility of a remote radiative cooling scheme in INTOR is discussed in Section 3 employing a volume integration technique of the radiation power along the scrape-off field line. The conclusions are summarized in Section 4.

2. REMOTE RADIATIVE COOLING IN D-III

2.1 Experimental Results on Remote Radiative Cooling

At the last IAEA meeting in Brussels, we reported that the divertor den-sity, $\overline{n}_{eDIV}$, increased non-linearly with the main plasma density [2] (Fig. 1). The maximum line-averaged divertor density obtained is ~ 2 x 10^{13} cm^{-3} (ℓ = 67 cm). Taking into account the fact that the separatrix surface is ~ 10 cm away from the wall, which is in good agreement with the location of the peak H_α line emission, the effective interferometer divertor plasma path-length is only ~ 20 -30 cm. Therefore, the electron density in the divertor is ~ 5 x 10^{13} cm-3. Moreover, since beam refraction problems have occurred for $\overline{n}_{eDIV}$ higher than 2 x 10^{13} cm^{-3} (ℓ = 67 cm), the electron density of the divertor is locally higher than 5 x 10^{13} cm^{-3}.

At the same time, the emission of the H_α line is strongly localized at the divertor, and increases non-linearly with respect to the line average density of the main plasma (Fig. 1). The particle confinement time in the divertor region, deduced from H_α line intensity and ionization rates [6], is ~ 1 msec. This value is in reasonable agreement with the lifetime of protons lost to the divertor wall with the flow velocity along the scrape-off field lines of 0.3 Cs [7] (Cs is the ion acoustic speed). The strong recycling and accumulation of particles in the divertor region during high density operation is consistent with radiative cooling of the divertor plasma, which will be discussed in the next section, and a reduction of the attenuation length of neutral hydrogen particles produced at the wall with the increase of

plasma density in the divertor region: $\lambda \sim 10$ cm at $n_e = 1 \times 10^{13}$ cm^{-3} and $\lambda < 3$ cm at $n_e \geq 5 \times 10^{13}$ cm^{-3} with $T_e \sim$ several eV. This phenomenon observed in Doublet III, which is a relatively large device ($a \sim 40$ cm), is significantly different from that observed in a small device, such as DIVA ($a \sim 10$ cm), where a linear relation between $\bar{n}_e$ and $n_{e_{DIV}}$ was observed.

Measurements by a 21-channel bolometer array indicate that the radiation power in the divertor volume increases significantly with increasing bulk plasma density and accounts for as much as 50% of the joule input power in high density discharges (Fig. 2). However, the radiation power in the main plasma increases only from 20 to 30% of the joule input power as the plasma density is increased from 1.5 to 5×10^{13} cm^{-3}. As a result, the heat load to the divertor plate is significantly reduced in high density operation. In Fig. 3, the peak heat load to the divertor plate (measured by IR camera) is observed to decrease as the radiation power in the divertor increased. The electron temperature in the divertor plasma is estimated to be ~ 7 eV from the two-dimensional TV observation of the OII line emission.

The source of this radiation power in the divertor is experimentally inferred to be the combination of the line radiation of hydrogen neutrals and oxygen. The Lyman series radiation power density estimated from the absolute intensity measurement of the H_α line is ~ 0.3 W/cm^3, and is in good agreement with the bolometer measurement. From a simple non-coronal equilibrium calculation of oxygen radiation (see Appendix), 0.3 W/cm^3 may be explainable by 1% oxygen in a plasma of $n_e = 5 \times 10^{13}$ cm^{-3} and $T_e = 5$ eV. Since Z_{eff} of the main plasma is ~ 1.1 -1.5, an oxygen concentration of $\sim 1\%$ in the divertor volume is reasonable.

2.2 Physical Model of Radiative Divertor Plasma

This process of radiative cooling in the divertor plays an important role in the formation of a dense and cold ($n_e \gtrsim 5 \times 10^{13}$ cm^{-3}, $T_e \lesssim 10$ eV) divertor plasma. A one-dimensional heat flow equation along the scrape-off field line with radiative cooling, $P_{r_{DIV}}$, is solved and the result shows a sufficient cooling of the divertor plasma [5]. The equations are [8]

$$\nabla_{\parallel} (K_{\parallel} \nabla_{\parallel} T_e) = P_{r_{DIV}}$$

$$\nabla_{\parallel} (n_e T_e) = 0 .$$

Here, we only include the radiation power of oxygen (see Appendix) in $P_{r_{DIV}}$. The boundary conditions for heat flow are:

$-Bp/B_T \bullet S K_{\parallel} \nabla_{\parallel} T_e = P_{OH} - P_r$ at the main plasma,

$-K_{\parallel} \nabla_{\parallel} T_e = \gamma \Gamma T_e$ at the divertor plate,

where $K_{\parallel}$ is the parallel electron heat conduction coefficient,

S is the cross sectional area of the divertor scrape-off,

γ is the heat transmission coefficient (= 7.8)

and the particle flux $\Gamma = 0.3\ Cs\ n_e$ [9].

Figure 4 is a typical computational result showing the T_e, n_e, and $P_{r_{DIV}}$ profiles along the field line for 1% oxygen level and $P_{OH} - P_r = 300$ kW. For an electron density at the separatrix of the main plasma of $n_{e_b} = 1.2 \times 10^{13}$ cm^{-3} ($\bar{n}_e \sim 5 \times 10^{13}$ cm^{-3}), the average $P_{r_{DIV}}$ attains ~ 0.3 W/cm^3. The divertor plasma is cooled from 27 eV near the main plasma down to 1 eV at the

divertor plate, while the density near the divertor plate exceeds 5×10^{13} cm^{-3}. The total remote radiation power is $\approx$ 80% of $P_{OH} - P_r$. This is compared with a lower plasma density case, $n_{e_b} = 0.4 \times 10^{13}$ cm^{-3} ($\bar{n}_e \sim 2 \times 10^{13}$ cm^{-3}), in which n_e and T_e are approximately constant along the field line. This simple calculation clearly shows the effectiveness of radiative cooling in the formation of a dense and cold divertor plasma.

3. FEASIBILITY OF REMOTE RADIATIVE COOLING IN INTOR

A method of integrating the radiation power along the field line is presented in this chapter and is utilized to estimate the impurity concentration in the divertor necessary to dissipate the power which flows from the main plasma into the divertor for typical INTOR parameters. Here, we use MKS units and eV for temperature. The heat conduction equation along the field line is

$$Q = -K_{\parallel} \frac{dT}{dx} \tag{1}$$

$$\frac{dQ}{dx} = -P_{r_{DIV}} \tag{2}$$

where Q is the heat flux density,

T is the electron temperature,

x is the coordinate along the field line.

From equations (1), (2), we get

$$\frac{Q_a^2}{2} - \frac{Q_b^2}{2} = \int_{T_b}^{T_a} K_{\parallel} P_{r_{DIV}} \, dT$$

where the subscripts a, b represent the main plasma edge, and the divertor plate, respectively.

Here,

$$K_{\parallel} = K_o \, T^{\frac{5}{2}} \qquad (K_o = 1.25 \times 10^3 \ \mathrm{W/m} \ / \ (\mathrm{ev})^{7/2})$$

and

$$P_{r_{DIV}} = n \, n_z \, L(T)$$

$$= n^2 f L(T)$$

$$= p^2 \, f \, \frac{L(T)}{T^2}$$

where n is the electron density,

n_z is the impurity density,

L(T) is the radiative cooling rate,

f is n_z/n,

p is the electron pressure,

we make the following two assumptions:

1) p is constant along the field line

2) f is constant along the field line

then we obtain

$$Q_a^2 - Q_b^2 = p^2 f \, (g(T_a) - g(T_b)) \tag{3}$$

where

$$g(T) = 2K_o \int_o^T L(T) \sqrt{T} \, dT$$

L(T) can be calculated once $n\tau$ (τ is the recycling time) is specified (see Appendix).

Figures 5 and 6 show the values of g(T) for oxygen and argon. From these figures it is seen that for $T_a > 40$ eV, and $T_b < 10$ eV, $g(T_a) >> g(T_b)$. Therefore, if $T_a > 40$ eV, $Q_a >> Q_b$, and $Q_a^2 \sim p^2 f \, g(T_a)$, T_b becomes low ($\lesssim$ 10 eV), and n_b becomes high.

Let us define f_o ;

$$f_o = \frac{Q_a^2}{p^2 \, g(T_a)} \tag{4}$$

From eq. (4), we can calculate the impurity concentration f_o that is necessary to radiate ~ 100% of the power from the main plasma Q_a, and to make a dense and cold divertor plasma.

We shall take the following as typical parameters for the INTOR divertor plasma:

R = 5 m (major radius)

P = $P_\alpha - P_r$ = 80 MW (power from the hot core)

d = 1 m (length of the divertor)

δ = 0.15 m (thickness of the scrape-off layer)

Θ = B_p/B_t = 0.05 (pitch of the field line)

n_a = 5×10^{19} m^{-3} (electron density at the divertor entrance)

$$Q_a = \frac{P}{4\pi R\delta\Theta} = 1.7 \times 10^8 \ W/m^2$$

$$\ell = \frac{d}{\Theta} = 20 \ m$$

ℓ is the distance from the main plasma edge to the divertor plate along the field line.

T_a is approximately given by [10]

$$T_a \simeq \left(\frac{7}{2}\ \frac{Q_a}{K_o}\ \ell\right)^{\frac{2}{7}} \simeq 100 \ eV$$

$$p = n_a T_a = 5 \times 10^{21} \ m^{-3} \ eV.$$

If we choose $n\tau$ to be 10^{17} $m^{-3} \cdot s$,

$$f_o = \frac{Q_a^2}{p^2\, g(T_a)} = 3.3\% \text{ for oxygen, } 1.6\% \text{ for argon.}$$

Next, the parameter dependence of f_o on n_a, $n\tau$, and δ are studied, because these quantities are difficult to predict with good accuracy.

Figures 7 and 8 show the dependence of f_o on n_a, and $n\tau$. The dependence on n_a is

$$f_o \propto \frac{1}{n_a^2}$$

The recycling time τ is short for the intensive recycling condition. For a smaller $n\tau$, the ionization stage is lower, which enhances L(T). The dependence of f_o on $n\tau$ is approximately $\propto (n\tau)^{0.3}$.

The f_o values scale like $\propto \delta^{-1.4}$ as shown in Fig. 9 (oxygen) and Fig. 10 (argon). The scaling is explained as follows

$$T_a \propto \delta^{\frac{2}{-7}} \text{ since } Q_a \propto \delta^{-1}, \text{ and } T_a \propto Q_a^{\frac{2}{7}}$$

$$f \propto \frac{Q_a^2}{T_a^2}\, g(T_a)^{-1}$$

Accordingly,

$$f \propto \delta^{-2} \cdot \frac{4}{\delta^{7}} \simeq \delta^{-10/7}$$

as g(T) is almost constant for $40 < T_a < 100$ eV.

The calculational results on INTOR are summarized as follows: If we allow 3% oxygen into the divertor, it is possible to radiate ~ 100% of the power flow into the divertor by oxygen line radiation under a condition of $n\tau \lesssim 10^{17}$ m^{-3} · s , $n_a \gtrsim 4 \times 10^{19}$ m^{-3}, $\delta \gtrsim 15$ cm. If we allow the argon impurity concentration to be ~ 3% in the divertor, argon will radiate ~ 100% of the power flow into the divertor under a condition of $n\tau \lesssim 10^{18}$ m^{-3} · s , $n_a \gtrsim 4 \times 10^{19}$ m^{-3}, $\delta \gtrsim 5$ cm.

It is necessary to note that our model is preliminary in the sense that we do not include hydrogen neutral recycling and radiation. The inclusion of this effect will cut down the f_o values obtained in this report.

4. CONCLUSIONS

The summary is given as follows:

1) In the Doublet III single-null poloidal divertor experiments, the radiation power from the hydrogen and oxygen becomes strong in the divertor for increasing electron density and accounts for as much as ~ 50% of the joule input power into the main plasma in high density operation.

2) As a result, the heat load to the divertor plates is reduced and a high density ($n_e \geq 5 \times 10^{13}$ cm^{-3}), low temperature ($T_e \lesssim 10$ eV) divertor plasma is formed.

3) A 1-D heat conduction calculation with oxygen line radiation shows good agreement with experimental results.

4) A simple calculation on the INTOR divertor shows that remote radiative cooling is possible with oxygen or argon.

Acknowledgement

The authors would like to acknowledge the JAERI and GA staffs for their experimental assistance and fruitful discussions. We gratefully acknowledge Dr. T. Ohkawa, Dr. M. Yoshikawa, and Dr. S. Mori for their continuous encouragement throughout this work.

4. CONCLUSIONS

The summary is given as follows:

1) In the Doublet III single-null poloidal divertor experiments, the radiation power from the hydrogen and oxygen becomes strong in the divertor for increasing electron density and accounts for as much as ~ 50% of the joule input power into the main plasma in high density operation.

2) As a result, the heat load to the divertor plates is reduced and a high density ($n_e \geq 5 \times 10^{13}$ cm^{-3}), low temperature ($T_e \lesssim 10$ eV) divertor plasma is formed.

3) A 1-D heat conduction calculation with oxygen line radiation shows good agreement with experimental results.

4) A simple calculation on the INTOR divertor shows that remote radiative cooling is possible with oxygen or argon.

Acknowledgement

The authors would like to acknowledge the JAERI and GA staffs for their experimental assistance and fruitful discussions. We gratefully acknowledge Dr. T. Ohkawa, Dr. M. Yoshikawa, and Dr. S. Mori for their continuous encouragement throughout this work.

APPENDIX

Calculation of Non-coronal Radiative Cooling Rate of Oxygen

The radiative cooling rate by oxygen is calculated as follows. The rate equations are:

$$- n_e n_j S_j + n_e n_{j-1} S_{j-1} - n_e n_j \alpha_j + n_e n_{j+1} \alpha_{j+1} - \frac{n_j}{\tau} = 0$$

(j = II, III ... VIII)

$$n_e n_{VIII} S_{VIII} - n_e n_{IX} \alpha_{IX} - \frac{n_{IX}}{\tau} = 0$$

$$\sum_{j=I}^{IX} n_j = n_{ox}$$

where subscript j : ionization stage (j = II means + 1 ion),

n_e : electron density,

n_j : oxygen particle density in the ionization stage j,

S_j : ionization rate from j ion to (j+1) ion,

α_j : recombination rate from j ion to (j-1) ion (sum of radiative recombination and dielectronic recombination),

τ : recycling time (assumed to be the same for all ions),

n_{ox} : total oxygen density.

With T_e, n_e, τ given, the fraction of each ionization stage f_j (= n_j/n_{ox}) is calculated, and the total radiative cooling rate L is given by:

$$L = \sum_{j=1}^{IX} f_j L_j \quad \left(= \frac{P}{n_e n_{ox}} \right)$$

where L_j is the radiative cooling rate for ions in the ionizaiton stage j (sum of excitation loss, ionization loss, and recombination loss), P is the total radiative power of oxygen. The ionization, recombination, and radiative cooling rates are calculated by a multi-ion species code [11]. The calculated L is shown in Fig. 11. L is calculated for $n_e = 1 \times 10^{14}$ cm^{-3}, $2eV < T_e < 1$ keV, τ = 0.1 ms, 1 ms, ∞ (coronal equilibrium). The coronal equilibrium calculation by Tarter [12] is also shown in the figure.

References

[1] NAGAMI, M., SHIMADA, M., YOKOMIZO, H., SEKI, S., KONOSHIMA, S., et al., Nucl. Fusion 18 (1980) 1325.

[2] NAGAMI, M., FUJISAWA, N., IOKI, K., KITSUNEZAKI, A., KONOSHIMA., S., et al., in Plasma Physics and Cotrolled Nucl. Fusion Research, (Proc. 8th Intern. Conf. Brussels, 1980) Vol. 2, IAEA, Vienna (1981) 367.

[3] NAGAMI, M., SHIMADA, M., et al., "Remote Radiative Cooling and Helium Ash Exhaustion with a Single-Null Poloidal Divertor in Doublet III", presented at the IAEA Technical Committee Meeting on Divertor and Impurity Control, Garching (1981).

[4] SHIMADA, M., IOKI, K., NAGAMI, M., YOKOMIZO, H., IZUMI, S., et al., "Suppression of Impurity Influx, Remote Radiative Cooling and Helium Ash Compression with Poloidal Divertor in Doublet III", presented at the 10th European Conf. on Controlled Fusion and Plasma Physics, Moscow.

[5] SHIMADA, M., NAGAMI, M., et al., Phys. Rev. Lett. 47 (1981) 796.

[6] JOHNSON, L. C., HINNOV, E., J. Quant. Spectrosc. Radiat. Transfer 13 (1979) 333.

[7] SHIMOMURA, Y., MAEDA, H., J. Nucl. Mater. 76 & 77 (1978) 617.

[8] TENNEY, F. H., LEWIN G., in "A Fusion Power Plant", Chap. 6 (ed. by Mills, R. G.) MATT-1050 (1974)

[9] KIMURA, H., MAEDA, H., UEDA, N., SEKI, M., KAWAMURA, H., et al., Nucl. Fusion 18 (1978) 1195.

[10] MAHDAVI, M. A., DeBOO, J. C., HSIEH, C. L., OHYABU, N., STAMBOUGH, R. D., and WESLEY, J. C., "Particle Exhaust from Discharges with an Expanded Boundary Divertor", Report No. GA-A16334, 1981 (unpublished). In this paper, the radiation power in the divertor is not explicitly taken into account in the discussion of the scrape-off plasma characteristics. However, a 1-D simulation similar to the one

described in [5] shows that T_a is well approximated by $\left(\frac{7}{2}\frac{Q_a}{K_o}\ell\right)^{\frac{2}{7}}$ even in a strong radiation case.

[11] HULSE, R., private communication. The atomic physics used in this code is the same as is described in POST, D. E., JENSEN, R. V., TARTER, C. B., GRASBERGER, W. H., and LOKKE, W. A., Atomic Data and Nuclear Data Tables 20 (1977) 397.

[12] TARTER, C. B., J. Quant. Spectrosc. Radiat. Transfer 17 (1977) 531.

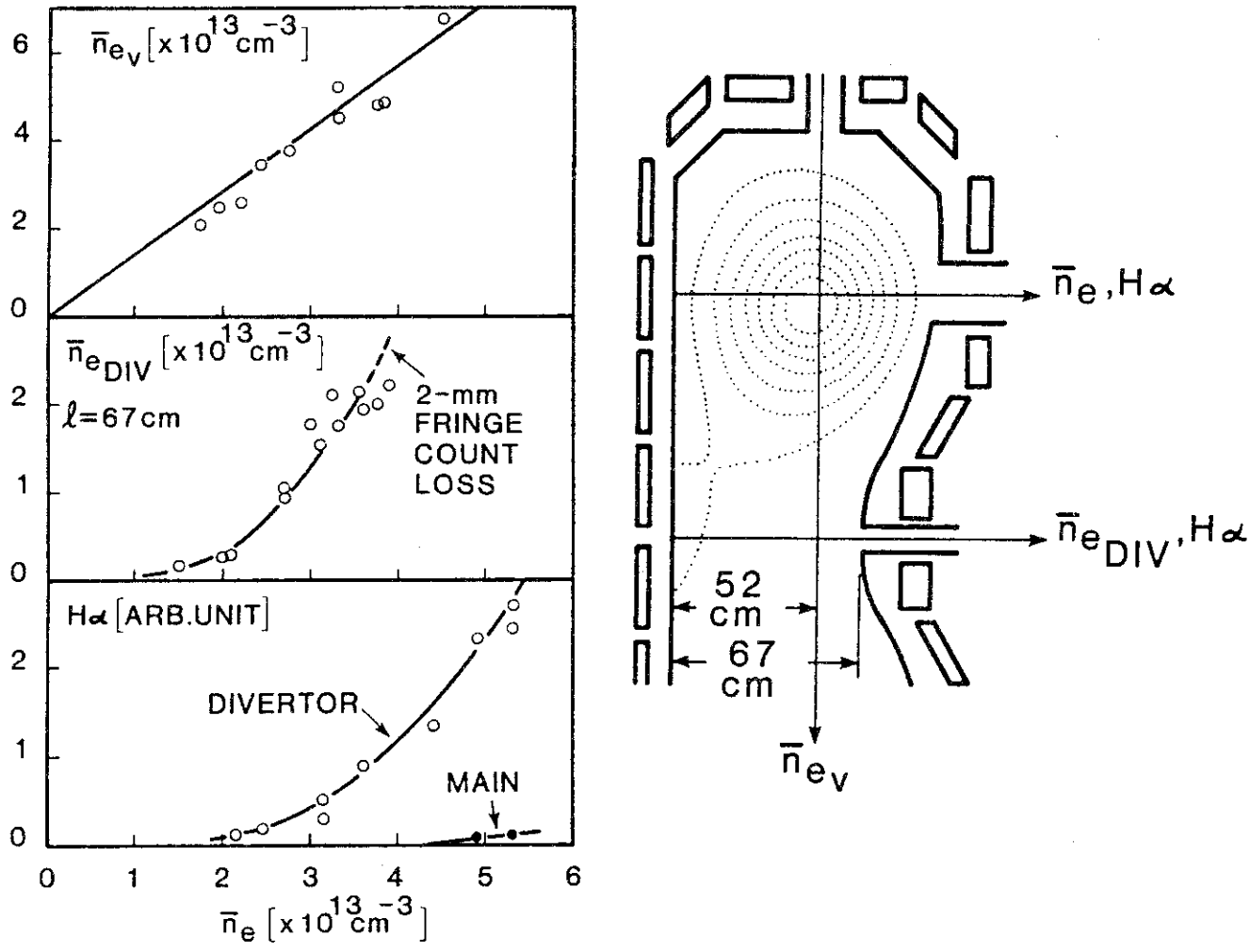

Fig.1 Vertical average density $\bar{n}_{ev}$, electron density at the divertor region (ℓ = 67 cm), and H_α line intensity along the central chord, and a chord through the divertor, vs. $\bar{n}_e$. Non-linear increase appears in $\bar{n}_{eDIV}$ and $H_{\alpha DIV}$ and not in $\bar{n}_{ev}$.

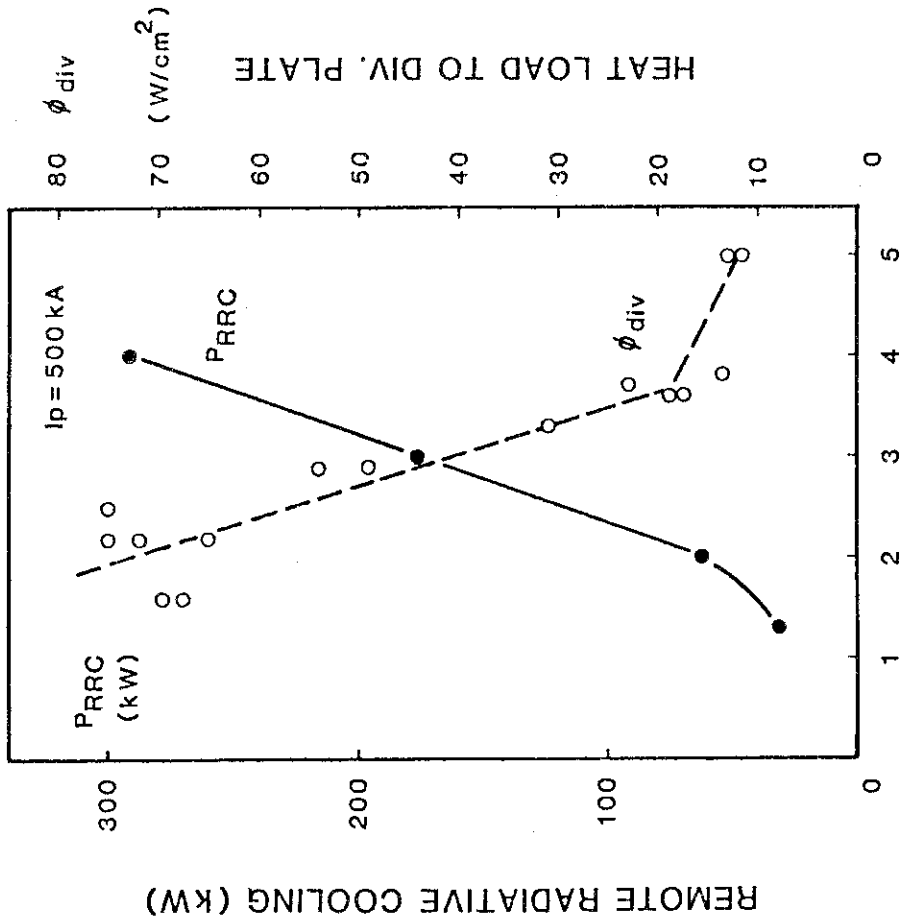

Fig.3 The peak heat load of the devertor plate ϕ_{DIV} is significantly reduced by the increase of remote radiative cooling power P_{RRC}.

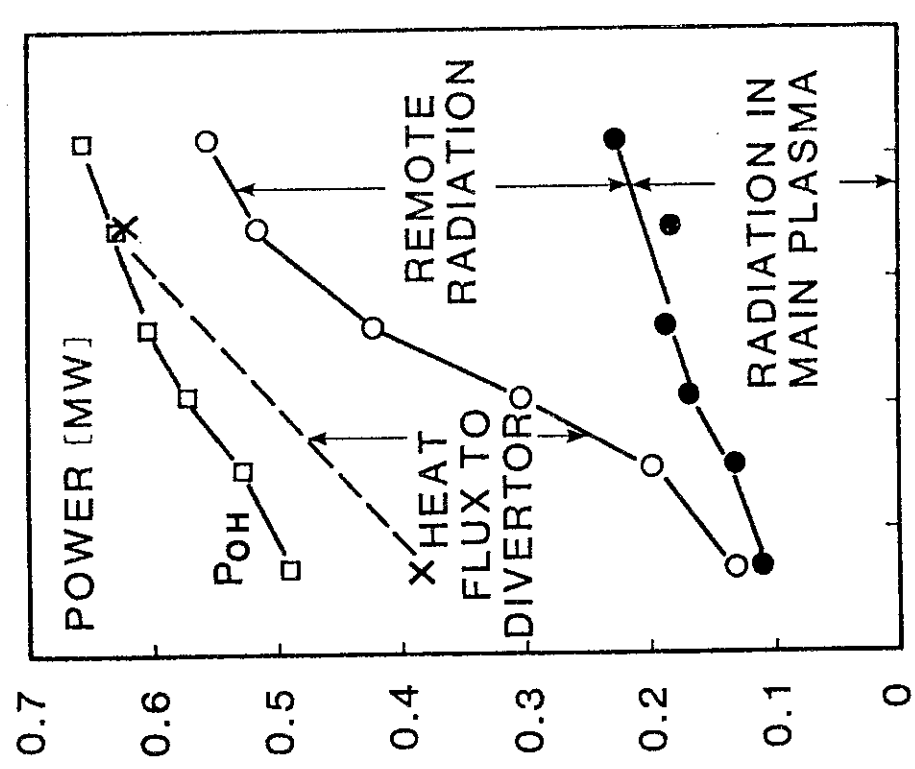

Fig.2 Power balance of diverted discharges of I_p = 500 kA. The remote radiation reaches ~50% of ohmic input at high n_e.

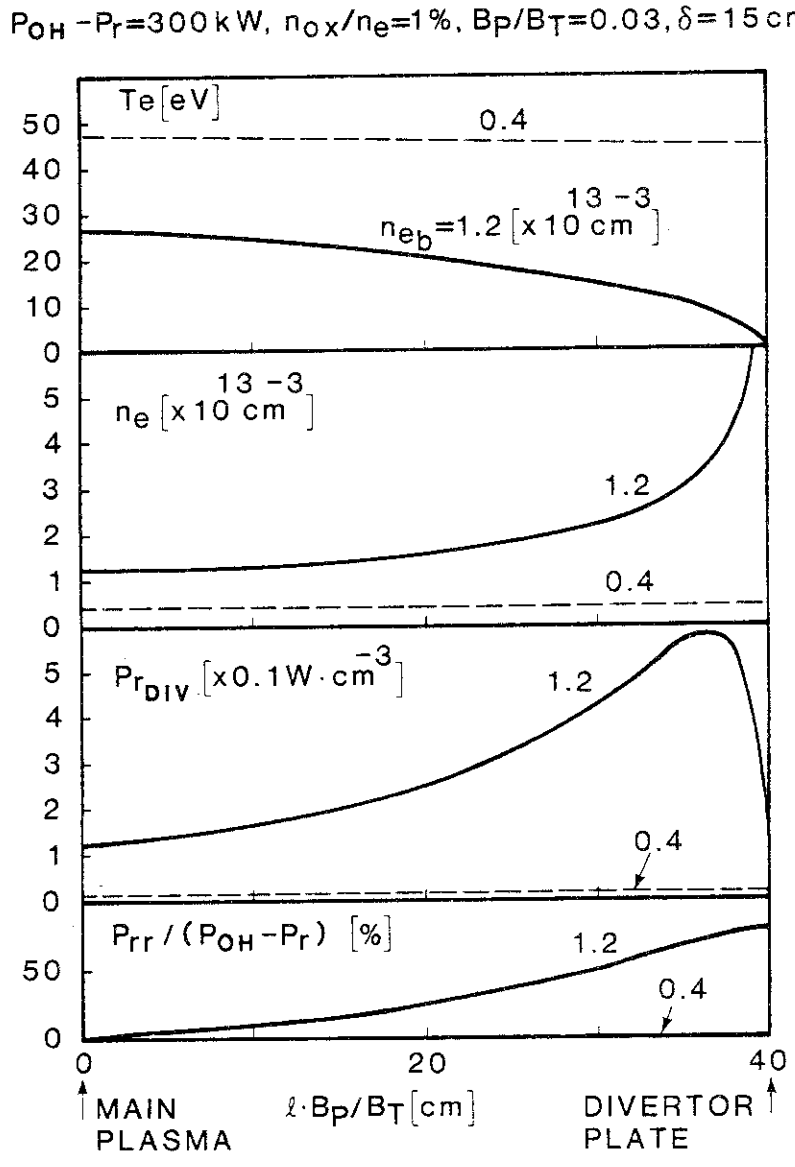

Fig.4 A simple calculation of one-dimensional heat flow along the scrape-off field line with remote radiation shows a sufficient cooling of the divertor plasma in high-n_e discharge.

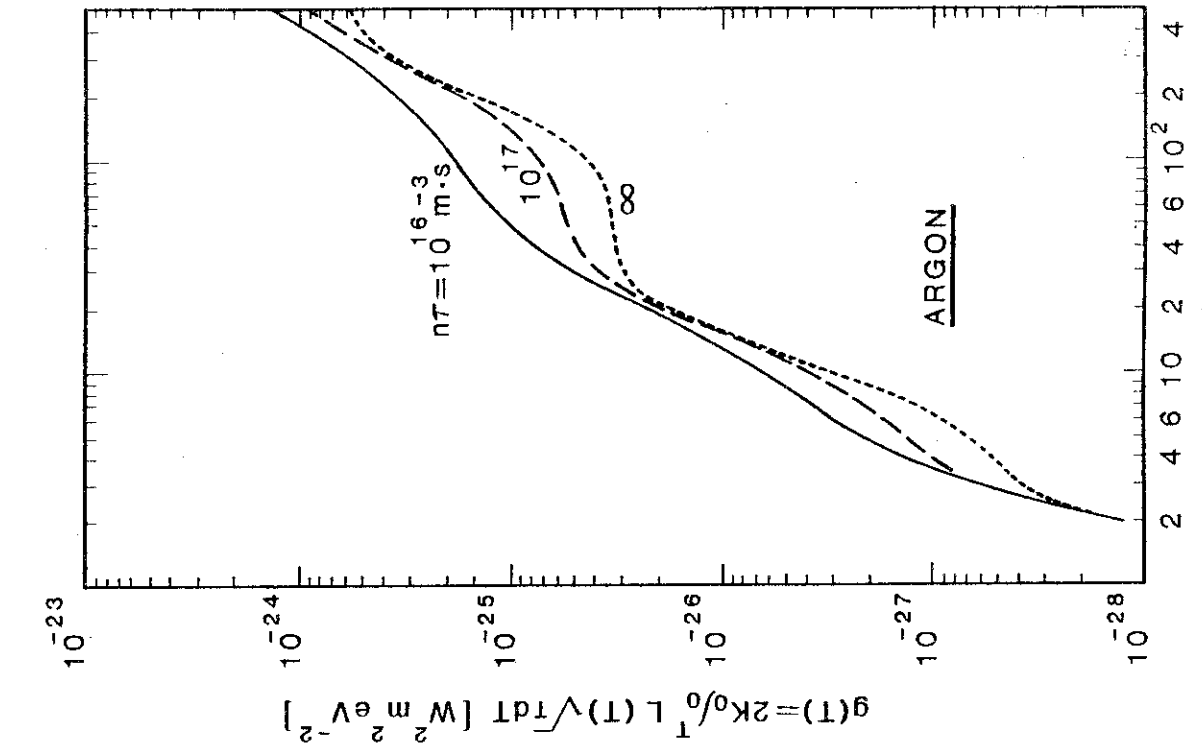

Fig.6 g(T) vs. T_e for argon.

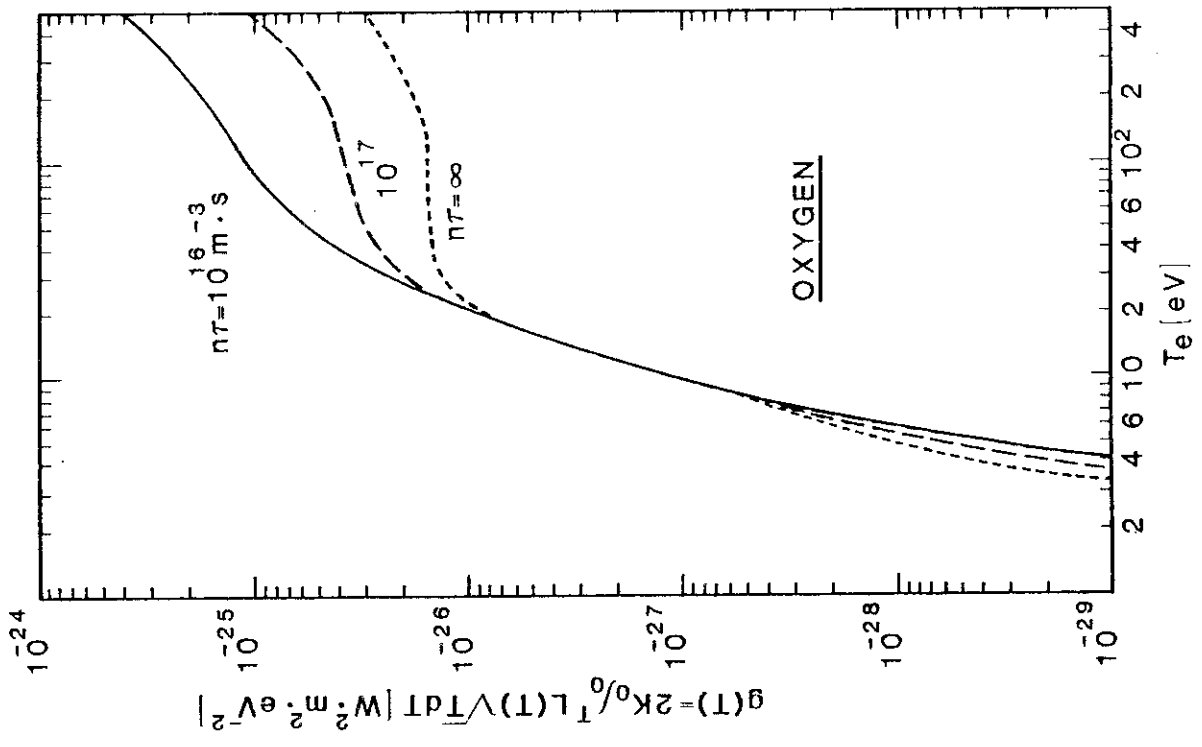

Fig.5 g(T) vs. T_e for oxygen. $n\tau$ is the electron density multiplied by the recycling time of the impurity particles.

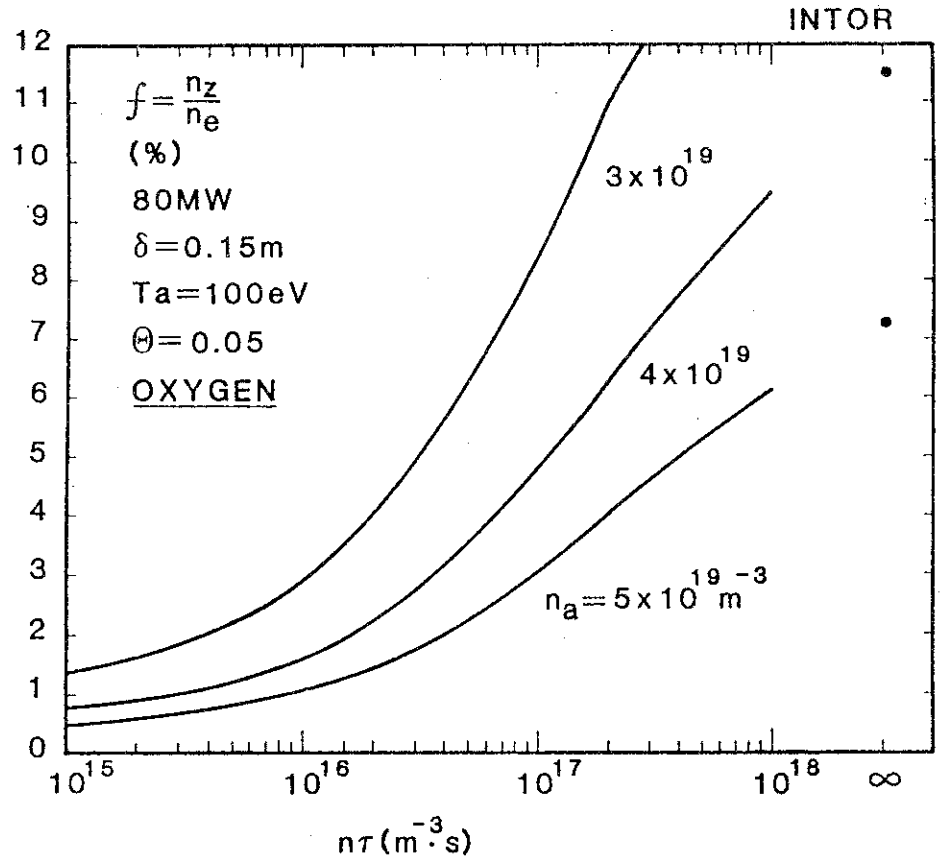

Fig.7 f vs. nτ (oxygen). f is the impurity concentration (= n_z/n_e) necessary to radiate ~100% of the heat flux from the main plasma. n_a is the electron density at the divertor entrance.

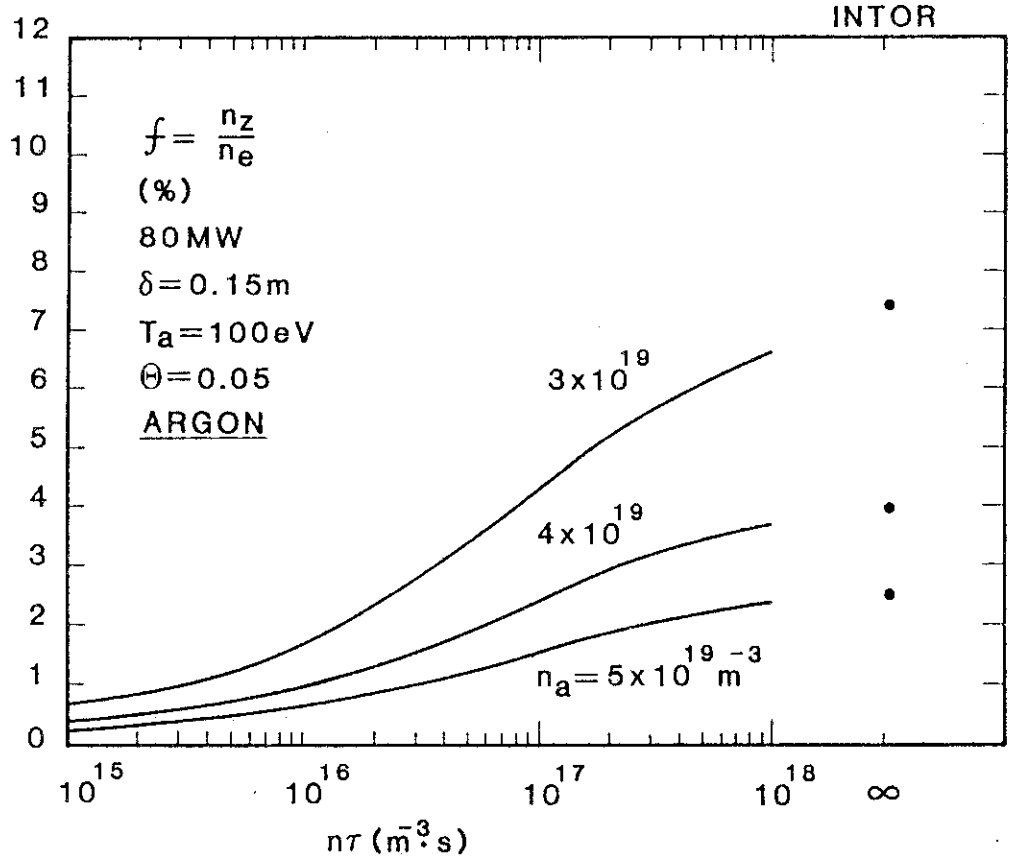

Fig.8 f vs. nτ (argon)

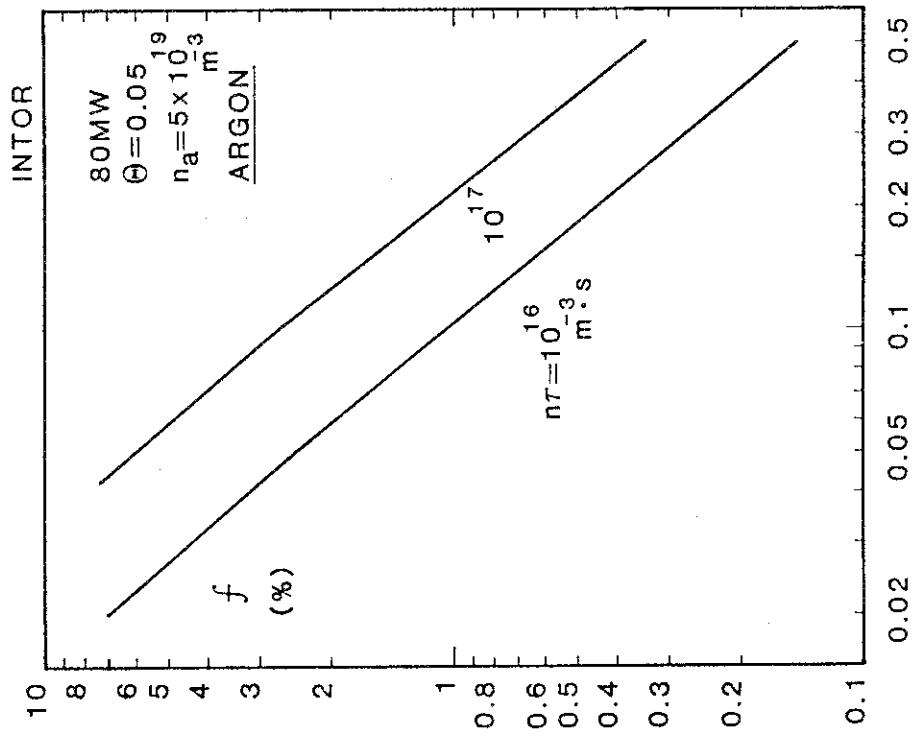

Fig.10 f vs. δ (argon).

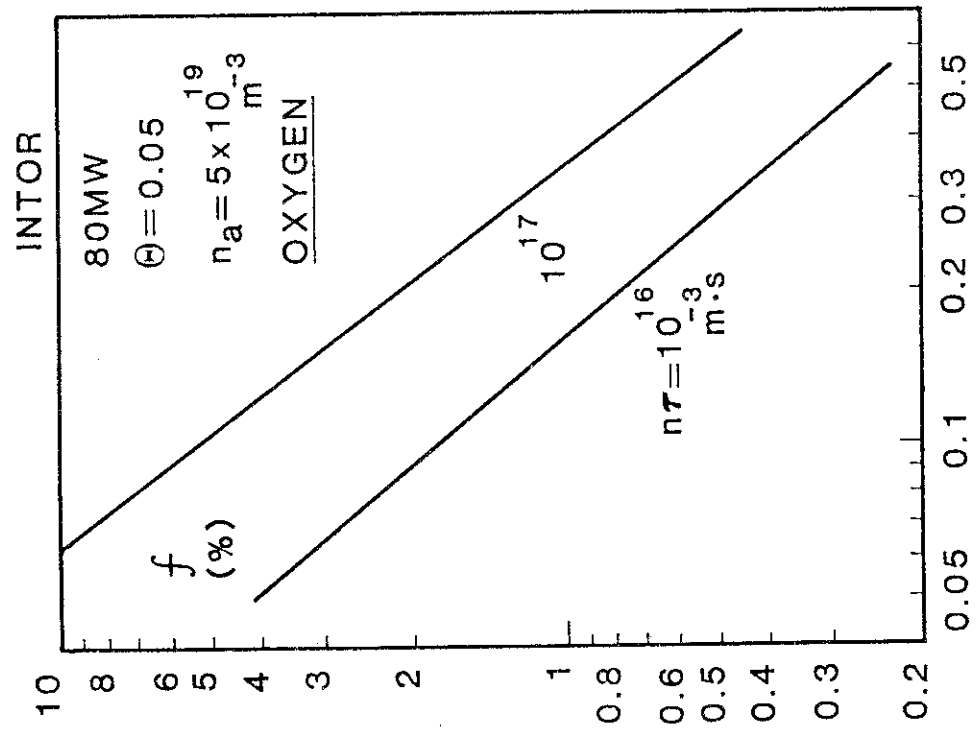

Fig.9 f vs. δ (oxygen). δ is the width of the scrape-off layer in the diverotr.

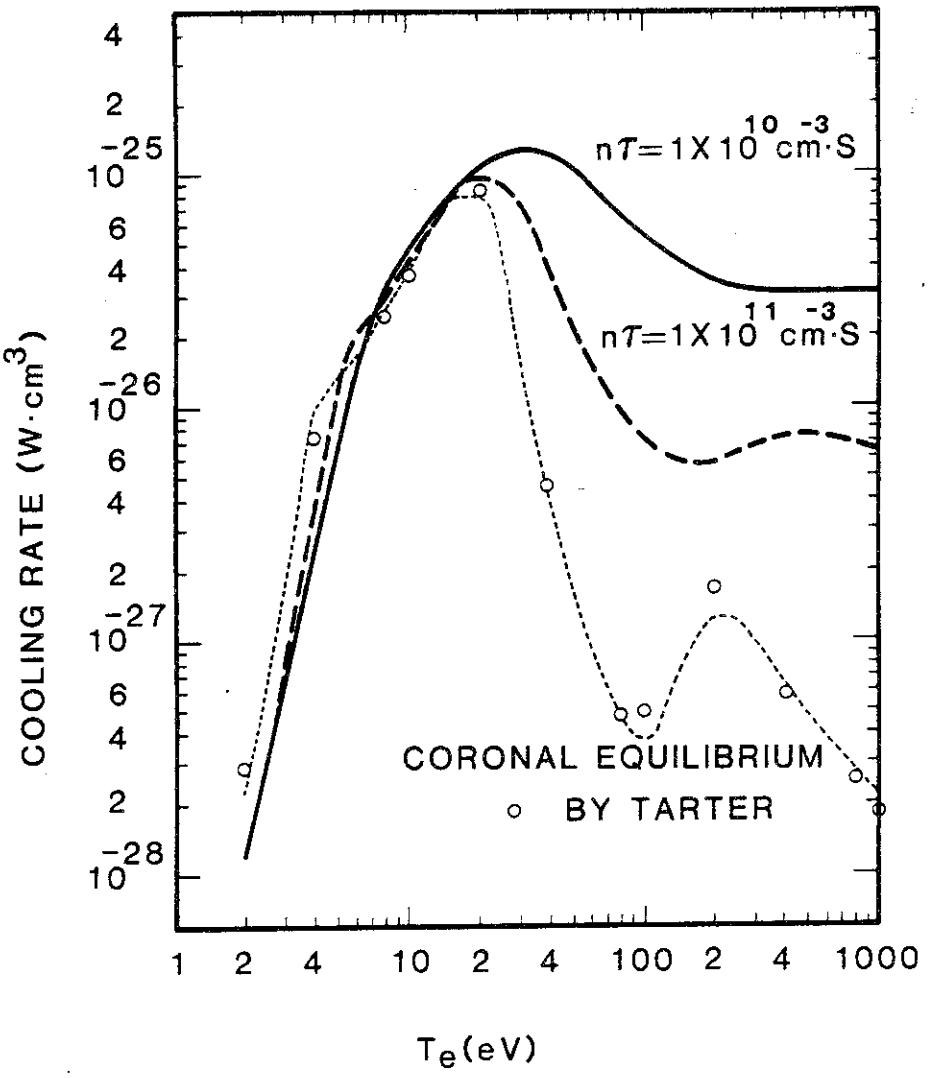

Fig.11 Non-coronal radiative cooling rate of oxygen.